URN (Paper): urn:nbn:de:gbv:ilm1-2014iwk-015:5

58th ILMENAU SCIENTIFIC COLLOQUIUM
Technische Universität Ilmenau, 08 – 12 September 2014
URN: urn:nbn:de:gbv:ilm1-2014iwk:3

QUASI-STATIC OBJECT SCANNING USING TECHNICAL VIBRISSAE

Christoph Will‡ */ Joachim Steigenberger*¶ */ Carsten Behn*‡

‡ Department of Technical Mechanics
Ilmenau University of Technology
Max-Planck-Ring 12 (Building F)
98693 Ilmenau, Germany
christoph.will@tu-ilmenau.de /
carsten.behn@tu-ilmenau.de

¶ Institute of Mathematics
Ilmenau University of Technology
Weimarer Straße 25
98693 Ilmenau, Germany
joachim.steigenberger@tu-ilmenau.de

ABSTRACT

Biological observations have shown that rodents use their vibrissae to estimate obstacle contact within a few contacts of the tactile hair. Based on this observation, a mechanical model of an animal vibrissa is developed, resulting in a long slim beam with a clamp as support at one end. A sweep of the beam along a profile, with its boundary describable by a strictly convex function, exhibits two phases. A phase in which the beam contacts the profile at its tip and a phase in which the beam contacts the profile tangentially (between the tip and the base). An analysis of the problem results in a decision criterion for the reconstruction and in a formula for the contact point of the beam with the profile. This is new in literature. Based only on forces and moments at the support it is possible to reconstruct the profile.

Index Terms— vibrissa, mechanical contact, beam, bending, large deflections, profile reconstruction.

1. INTRODUCTION

Some mammals, e.g. mice and rats, have large tactile hairs in their snout region (mystacial vibrissae). These hairs allow the animal to get information about its environment. The information is processed in the support of the vibrissa, the follicle sine complex (FSC) as shown in Fig. 1. In it, mechanoreceptors (e.g. Merkel cells) convert mechanical strain into nerve signals for further processing. Observations in [8] show, that the animals are able to determine contacts with obstacles within a few touches of a vibrissa. The key observation here is, that the animal has only the information generated by the mechanoreceptors in the FSC.

This biological paragon — incorporating the vibrissa as a lever of force transmission and the support FSC as a processing unit of signals — is focus of main interest in, e.g., robotic research to develop artificial sensors. Based on this paragon we develop a mechanical model for object scanning. Before doing this, we focus on the state of art to get hints for developing and to make a dissociation of the actual work in this field.

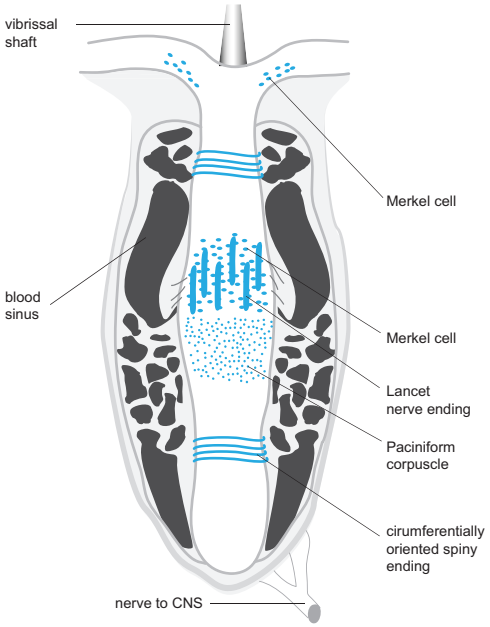

Figure 1: Follicle sine complex [2], arranged by D. Voges (TU Ilmenau).

2. STATE OF THE ART

Many different approaches were taken to transfer the well working biological system into the field of engineering for obstacle detection. Very simple models, like the one presented in [6] and shown in Fig. 2, use long thin beams to detect deformation due to obstacle contact on mobile robots. If the "whisker-like" sensor detects a deformation of the beam, the position is marked as containing obstacles. In this case the authors are not interested in any particular information about the obstacle, only in its existence to restrict the range of motion of the robot.

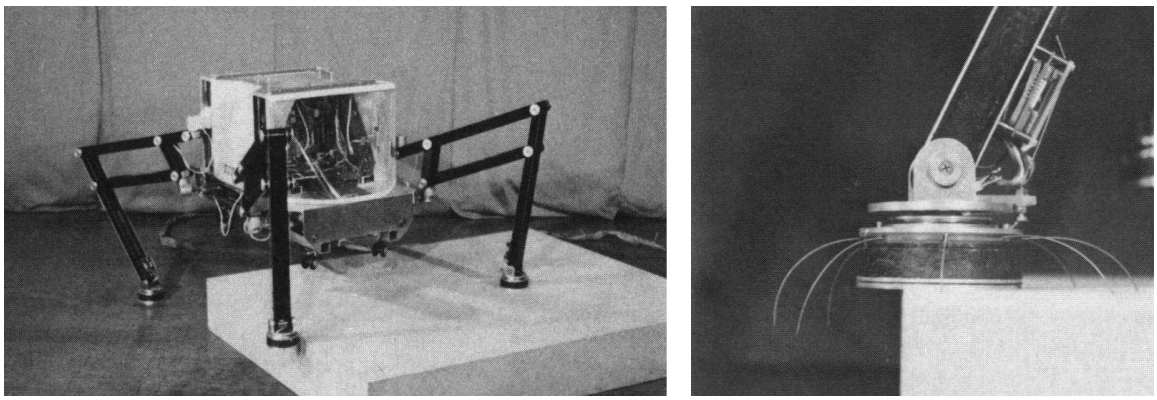

Figure 2: Mobile robot with whisker-like sensors, [6].

In [7] and [12] the approaches are similar, but the described methods focus on information about the object. This is obtained by using a method based on computer tomography in [12]. The beam can be seen as a ray and a deflection of the beam as ray distraction. Thus, it is possible to *estimate* the contact point based on the angle of deflection at the base of the beam. Principle and realization for this method are shown in Fig. 3. In [7] the linear theory of elasticity is applied to large deflections with angular relations shown in Fig. 4. Both methods have in common that only the deflection angle and no moments or forces are measured, which obviate the need of calibration for the sensors. Nevertheless, this needs a scanning tactic which ensures that the estimation of the deflection angle using linear theory is valid.

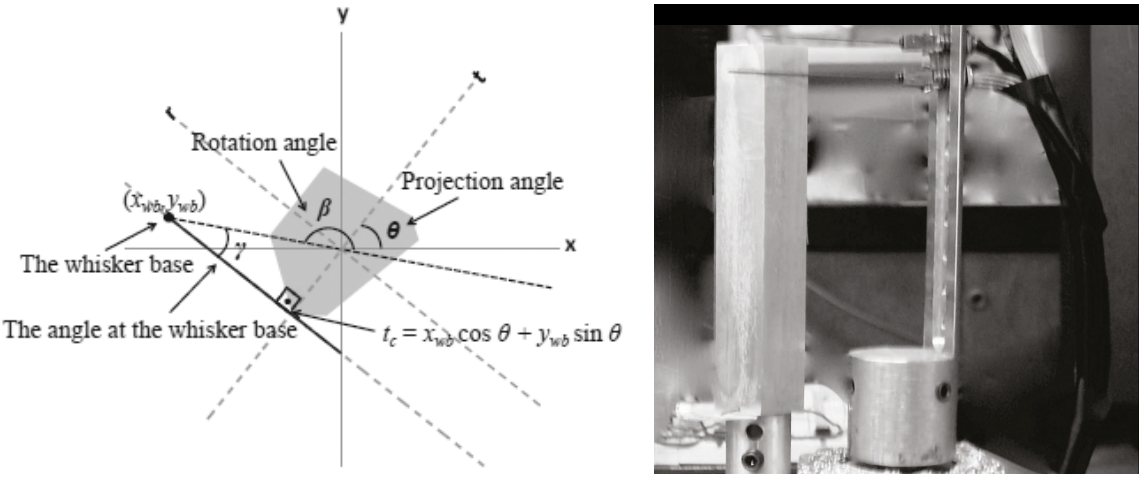

Figure 3: Model and prototype of obstacle detection using only angular relations, [12].

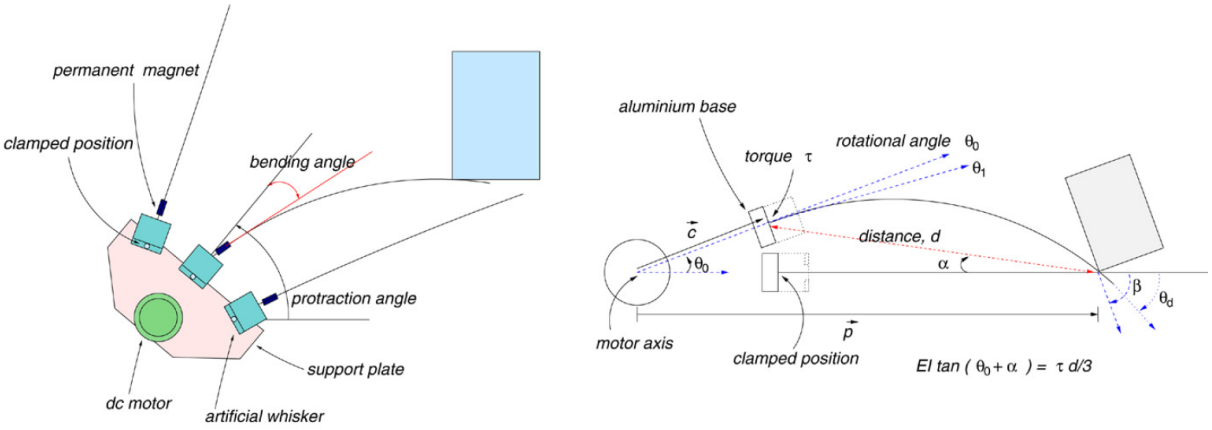

Figure 4: Model for obstacle distance detection using only the bending angle, [7].

A model which includes small deformations and the curvature of the vibrissa is presented in [3]. As shown in Fig. 5, the authors added the curvature and the linear deflection of the beam to get the actual position of the beam. The achievable accuracy of the model depends on the precurvature of the beam, because the curvature is assumed to be a function of the beam axis shown in Fig. 5B.

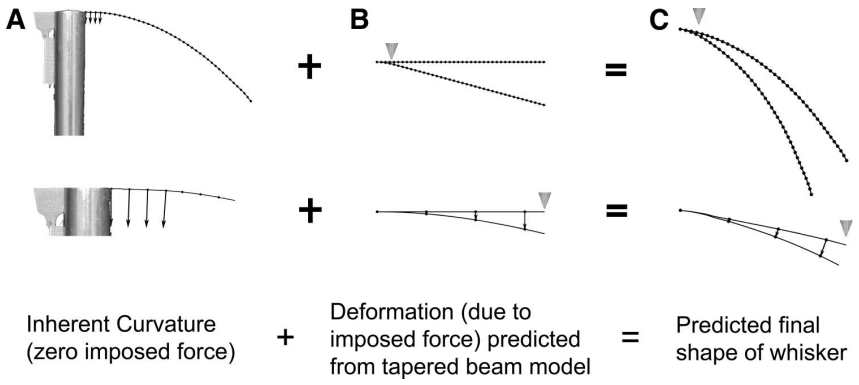

Figure 5: Proposed method to consider small deflections of pre-curved beams from [3].

A method, which considers large deflections and focuses on object detection, is proposed in [10] for plane problems and in [4] for spacial problems. In both works, the authors relinquish the linear approximation of the curvature and express the problem in natural coordinates, thus allowing large deflections of the beam and a clear formulation of

the boundary conditions. Both are also only interested in reconstructing the profile from experimental data, thus no analysis on how to compute the reactions at the clamp for a verification of the system takes place. The mechanical model used in [10] is shown in Fig. 6 and the result of the reconstruction in Fig. 7.

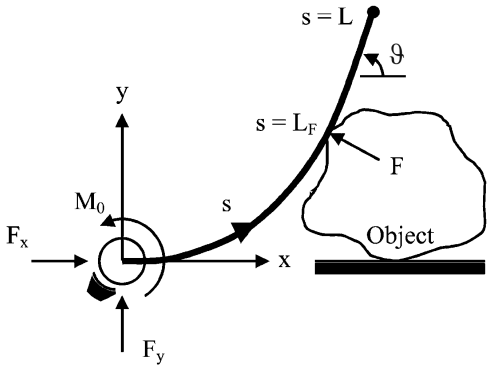

Figure 6: Mechanical model regarding large deflection due to the contact with a rigid body, [10].

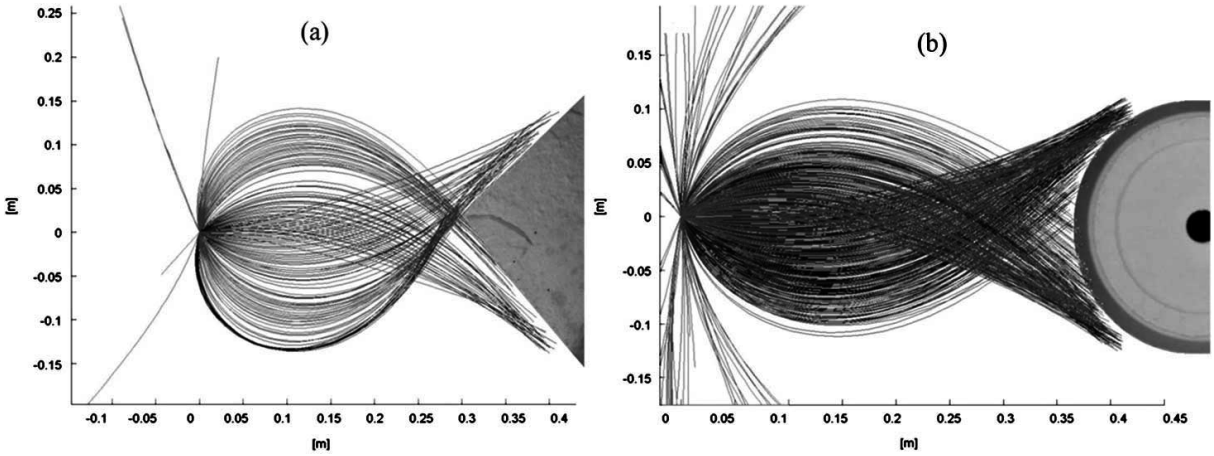

Figure 7: Deformed beams gained from experimental data: (a) triangle profile, (b) circle profile; [10].

Others, like [9], approximate the curvature using finite differences. This gives an option to consider the curvature of an undeformed biological vibrissa.

3. PROBLEM FORMULATION AND SOLUTION

The present paper deals with the problem what an animal "feels" and perceives by means of a single vibrissa while moving along an obstacle, and which information it can get about the obstacle. As already mentioned in Section 1, the only information is available at the support of the vibrissa. In order to get further information, we treat the problem analytically to the greatest extent. The work is based on [11] and [13]. In order to model the problem, the following assumptions are made:

- The animal is moving at low speed, this allows us to treat the problem quasi-statically.
- All movements take place in a plane, w.l.o.g. in the (x, y)-plane, along the x-axis with the base of the vertical vibrissa at $y = 0$.
- The vibrissa is assumed to be a long, slim, straight (until now, no precurvature is assumed) beam with constant second moment of area I_z, constant Young's modulus E and length L. Thus, ignoring shear stress, the Euler-Bernoulli theory for large deflections is applicable.
- Without loss of generality, the beam moves relative to the obstacle from the right to the left along the x-axis.

- The stress at each point of the beam is sufficiently small to describe the behavior of the material with Hooke's law of linear elasticity.

- The support of the beam is very stiff compared to the stiffness of the beam, thus it can be approximated as a clamp, whereby we know that this will not match the reality of the vibrissa. But our work is in the bionic point of view. We do not want to construct a prototype with 1-to-1 properties of the biological paragon. In upcoming works we will diminish the stiffness of the support to get hints, for which mechanical reasons the biological vibrissa is embedded in a compliant FSC support.

- The obstacle, responsible for a deflection of the beam, is a rigid body fixed in the (x, y)-plane with a strictly convex contour. Its boundary is described by the function $g : x \mapsto g(x)$. Furthermore, $g \in C^1(\mathbb{R}; \mathbb{R})$ is assumed.

- Deformation of the beam is caused by a single contact force (due to an object contact). This force is perpendicular to the obstacle profile, i.e., no friction forces are taken into account.

With these assumptions made above, the Euler-Bernoulli equation, first mentioned in [5], is applicable:

$$\kappa(s) = \frac{M_{bz}(s)}{EI_z}\,, \tag{1}$$

where $M_{bz}(\cdot)$ is the bending moment around the z-axis, $s \in [0, L]$ the arc length of the beam and $\kappa(\cdot)$ the curvature, see Fig. 8.

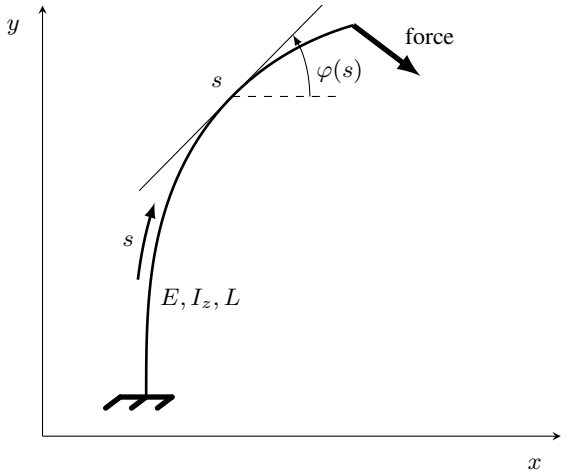

Figure 8: Euler-Bernoulli beam under large deflection.

To archieve a short notation of formulas we shall use dimensionless coordinates. For this end we use the units of measure [length] $= L$, [moments] $= EI_zL^{-1}$ and [forces] $= EI_zL^{-2}$ (so, e.g., we have $s = Ls^*\,,\ s \in [0, 1]$). From now on, all quantities are given in dimensionless representation, where we drop the asterisk for brevity in the following. Hence (1) becomes

$$\kappa(s) = M_{bz}(s)\,. \tag{2}$$

The deformed beam in the (x, y)-plane can now be given by

$$\begin{aligned}
\frac{\mathrm{d}}{\mathrm{d}s}x(s) &= \cos\left(\varphi(s)\right)\,,\\
\frac{\mathrm{d}}{\mathrm{d}s}y(s) &= \sin\left(\varphi(s)\right)\,,\\
\frac{\mathrm{d}}{\mathrm{d}s}\varphi(s) &= \kappa(s)\,.
\end{aligned}$$

In order to reach a short formulation of the problem, the profile function g needs to be parameterized. Because $g \in C^1$ is strictly convex, x and y become functions of the slope angle α in the following:

$$\begin{aligned} & \frac{\mathrm{d}}{\mathrm{d}x} g(x) = g'(x) = \tan(\alpha) \\ \Rightarrow \quad & x = \xi(\alpha) := g'^{-1}(\tan(\alpha))\,, \\ \Rightarrow \quad & y = \eta(\alpha) := g(\xi(\alpha))\,. \end{aligned}$$

Every point $(x, g(x))$ is now mapped to the tuple $(\xi(\alpha), \eta(\alpha))$. As a next step the boundary conditions have to be formulated. To do this the contact between beam and profile has to be seen in two phases, see Fig. 9:

- Phase A: Contact of beam tip and profile with $\varphi(1) \geq \alpha$,
- Phase B: Contact of a point $s_1 \in (0, 1)$ and the profile with equal angles $\varphi(s_1) = \alpha$.

In both phases, the contact point is given by the slope angle α of the profile.

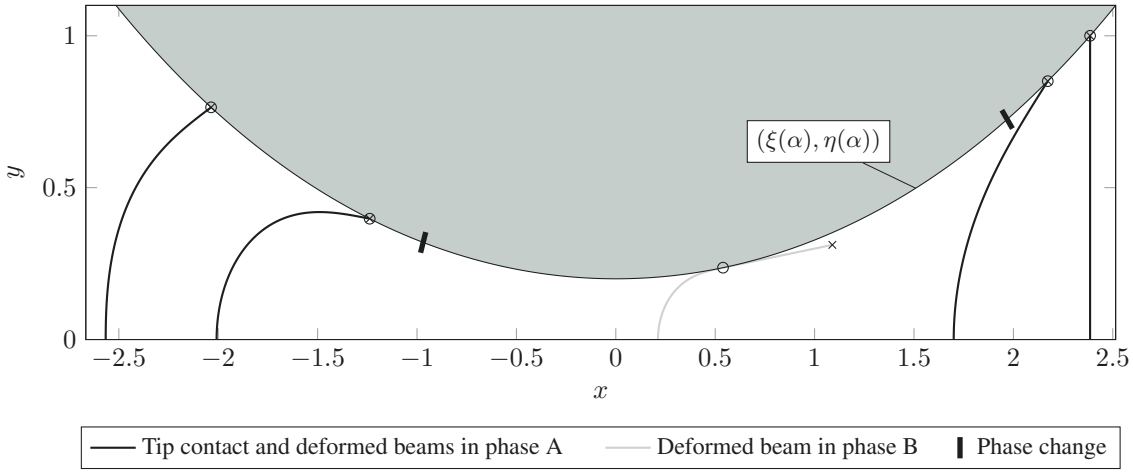

Figure 9: Profile with deflected beams.

3.1. Phase A: Contact at the tip

An equation for the bending moment results from the equilibrium of moments applied on the deformed state shown in Fig. 10:

$$\begin{pmatrix} 0 \\ 0 \\ 0 \end{pmatrix} = - \begin{pmatrix} 0 \\ 0 \\ M_{bz}(s) \end{pmatrix} + \left(\begin{pmatrix} x(1) \\ y(1) \\ 0 \end{pmatrix} - \begin{pmatrix} x(s) \\ y(s) \\ 0 \end{pmatrix} \right) \times \underbrace{f \begin{pmatrix} \sin(\alpha) \\ -\cos(\alpha) \\ 0 \end{pmatrix}}_{=\vec{F}}$$

$$\Leftrightarrow \quad M_{bz}(s) = f\Big(\big(y(s) - \eta(\alpha)\big) \sin(\alpha) + \big(x(s) - \xi(\alpha)\big) \cos(\alpha) \Big), \quad s \in (0, 1)\,. \tag{3}$$

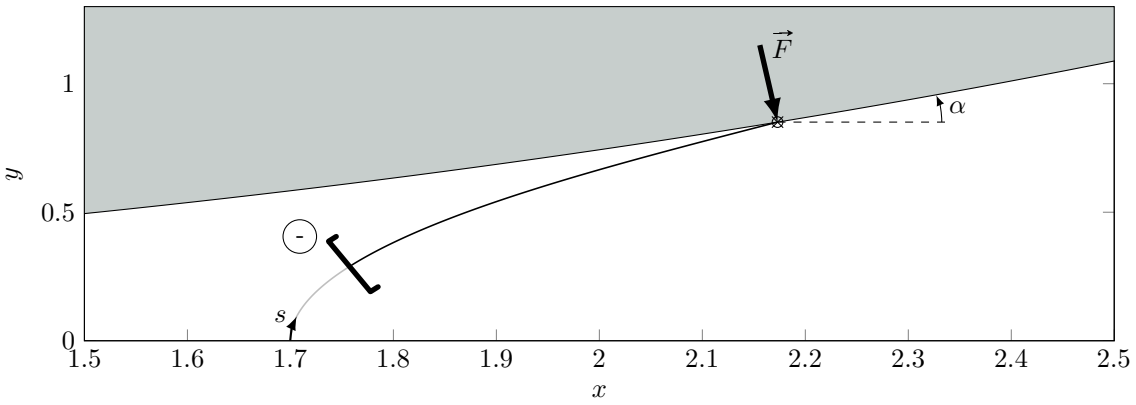

Figure 10: Deflected beam in Phase A.

In order to decouple the bending moment (i.e., the curvature $\kappa(\cdot)$, see (2)) from $x(s)$ and $y(s)$, the derivative of (3) with the additional boundary condition $\kappa(1) = M_{bz}(1) = 0$ is considered. This results in the following ODE system (4) with boundary conditions (5):

$$\boxed{\begin{array}{ll} \text{(a)} \quad \kappa'(s) = f\cos(\varphi(s) - \alpha) & \text{(c)} \quad x'(s) = \cos(\varphi(s)) \\ \text{(b)} \quad \varphi'(s) = \kappa(s) & \text{(d)} \quad y'(s) = \sin(\varphi(s)) \end{array}} \tag{4}$$

$$\boxed{\begin{array}{lll} \text{(a)} \quad \varphi(0) = \frac{\pi}{2} & \text{(c)} \quad \kappa(1) = 0 & \text{(d)} \quad x(1) = \xi(\alpha) \\ \text{(b)} \quad y(0) = 0 & & \text{(e)} \quad y(1) = \eta(\alpha) \end{array}} \tag{5}$$

This boundary value problem splits into two separate problems: {(4a,b),(5a,c)} and {(4c,d),(5b,d,e)}. The first one has

$$\kappa^2 = 2f\left(\sin(\varphi - \alpha) - \sin(\varphi_1 - \alpha)\right) \tag{6}$$

as a first integral with $\varphi_1 := \varphi(1)$.
The bending moment, considering the lower part of the beam, depends on the clamp reactions M_{Az}, F_{Ax}, F_{Ay}, which results in a first integral in the form

$$\kappa^2 = 2f\sin(\varphi - \alpha) - 2f\cos(\alpha) + M_{Az}^2\,.$$

Taken the numerical computation into account, a domain for the still unknown variable φ_1 would be advantageous. For this purpose (6) is rearranged:

$$\kappa^2 = 4f\sin\left(\frac{\varphi - \varphi_1}{2}\right)\cos\left(\frac{\varphi + \varphi_1 - 2\alpha}{2}\right)\,. \tag{7}$$

Hence $\kappa^2(s) \geq 0$ has to be fulfilled, three cases must to be discussed ($f > 0$):

1. At least one factor is equal to zero: Consequently $\kappa(s) \equiv 0$ holds. In this trivial case, the beam is not deformed at all and there is no need for further discussion.

2. Both factors are negative: The sine function is positive on the interval $(-\pi, 0)$ and negative on $(\pi, 2\pi)$. This results in the inequations

   $$-2\pi < \varphi(s) - \varphi_1 < 0 \quad \vee \quad 2\pi < \varphi(s) - \varphi_1 < 4\pi\,.$$

   Hence $\varphi(s) < \varphi_1 \ \vee \ \varphi(s) > 2\pi$. This is a **contradiction**, because $\varphi(s) \in \left[\varphi_1, \frac{\pi}{2}\right] \ \forall s \in [0, 1]$.

3. Both factors are positive: The sine function is positive on the domain $(0, \pi)$, the cosine function on $\left(-\frac{\pi}{2}, \frac{\pi}{2}\right)$. Therefore, it must hold:

   $$0 < \varphi(s) - \varphi_1 < 2\pi \quad \wedge \quad -\pi < \varphi(s) + \varphi_1 - 2\alpha < \pi\,.$$

The first inequality contains no additional information, the second one yields:

$$\begin{aligned} & \varphi(s) + \varphi_1 < \pi + 2\alpha \; \forall s \\ \Rightarrow \qquad & \varphi_1 < \frac{\pi}{2} + 2\alpha, \;\; \text{since} \;\; \varphi(s) \leq \frac{\pi}{2} \, . \end{aligned}$$

Therefore, the angle φ_1 has to be in the domain $\alpha < \varphi_1 < \min\left(\left\{\frac{\pi}{2}, \frac{\pi}{2} + 2\alpha\right\}\right)$.
With respect to the assumptions made at the beginning of this section, the curvature is non-positive along the solutions of (4a,b), hence we get

$$\frac{\mathrm{d}}{\mathrm{d}s}\varphi(s) = \kappa(s) = -\sqrt{2f}\sqrt{\sin(\varphi(s) - \alpha) - \sin(\varphi_1 - \alpha)} \tag{8}$$

as a ODE with separated variables for $\varphi(s)$. For the sake of brevity the function $\mathbb{H}_A$ is introduced:

$$\mathbb{H}_A : (t, u) \mapsto \mathbb{F}\left(\frac{\sin\left(\frac{\pi}{4} - \frac{t}{2}\right)}{\sin\left(\frac{\pi}{4} - \frac{u}{2}\right)}, \sin\left(\frac{\pi}{4} - \frac{u}{2}\right)\right) \, , \tag{9}$$

where $\mathbb{F}$ is the incomplete elliptic integral of first kind according to the definition [1, 17.2.7]

$$\mathbb{F} : (z, k) \mapsto \int_0^z \frac{1}{\sqrt{1 - \psi^2}\sqrt{1 - k^2\psi^2}} \, \mathrm{d}\psi \, .$$

Separation of variables applied on (8) with initial value (5a) yields:

$$\sqrt{f}s = \mathbb{H}_A\big(\varphi(s) - \alpha, \varphi_1 - \alpha\big) - \mathbb{H}_A\left(\frac{\pi}{2} - \alpha, \varphi_1 - \alpha\right) \, . \tag{10}$$

Hence the contact force f can be expressed as

$$f = \left(\mathbb{H}_A\left(\varphi_1 - \alpha, \varphi_1 - \alpha\right) - \mathbb{H}_A\left(\frac{\pi}{2} - \alpha, \varphi_1 - \alpha\right)\right)^2 =: f(\varphi_1, \alpha) \, . \tag{11}$$

Therefore, the only unknown parameter at this stage is the angle of the tip of the beam φ_1. To get a formula for this parameter, (5b,e) have to be considered, which can be done in two ways presented in the following sections.

3.1.1. Substitution of variable

Instead of letting the arc length s be the variable of the ODE system, $y(s)$ can also be expressed in terms of the slope angle:

$$\frac{\dfrac{\mathrm{d}y(s)}{\mathrm{d}s}}{\dfrac{\mathrm{d}\varphi(s)}{\mathrm{d}s}} = \frac{\mathrm{d}y(\varphi)}{\mathrm{d}\varphi} = \frac{1}{\kappa(\varphi)} \sin\left(\varphi\right) \, ,$$

with boundary conditions $y(\frac{\pi}{2}) = 0$ and $y(\varphi_1) = \eta(\alpha)$. At first, only the first condition is considered, which leads to

$$y(\varphi) = -\frac{1}{\sqrt{2f}} \int_{\frac{\pi}{2}}^{\varphi} \frac{\sin(\tau)}{\sqrt{\sin(\tau - \alpha) - \sin(\varphi_1 - \alpha)}} \, \mathrm{d}\tau \, .$$

The second boundary condition results in an implicit expression for $\varphi_1 \in \left(\alpha, \min\left\{\frac{\pi}{2}, \frac{\pi}{2} + 2\alpha\right\}\right)$:

$$\eta(\alpha)\sqrt{2f} + \int_{\frac{\pi}{2}}^{\varphi_1} \frac{\sin(\tau)}{\sqrt{\sin(\tau - \alpha) - \sin(\varphi_1 - \alpha)}} = 0 \, . \tag{12}$$

Note that the integral (12) can be analytically calculated, but not in short terms without using elliptic Jacobi functions. Anyway, we have — using (11) and (12) — an equation for $\varphi_1(\alpha)$ which is a little bit unpleasant. Therefore, it is convenient to switch to another method of solution in the next subsection.

3.1.2. Shooting method

Instead of substituting the variable, the problem can efficiently be solved by applying a shooting method for φ_1. Dependent on the implementation, this method can be both faster and more accurate.
Let $\varphi_1^* \in \left[\alpha + \epsilon, \min\left\{\frac{\pi}{2}, \frac{\pi}{2} + 2\alpha\right\} - \epsilon\right]$ be a valid candidate for φ_1. The corresponding deflection angle $\varphi(s)$ can be calculated from (10) with f from (11):

$$\varphi(s, \varphi_1^*) = \alpha + \mathbb{H}_A^{-1}\left(\sqrt{f(\varphi_1^*, \alpha)}s + \mathbb{H}_A\left(\frac{\pi}{2} - \alpha, \varphi_1^* - \alpha\right), \varphi_1^* - \alpha\right), \text{ with}$$
$$\mathbb{H}_A^{-1}(t, u) = -\frac{\pi}{2} + 2\arccos\left(\text{JacobiSN}\left(t, \cos\left(\frac{\pi}{4} + \frac{u}{2}\right)\right)\cos\left(\frac{\pi}{4} + \frac{u}{2}\right)\right)$$

from (9) and JacobiSN according to [1, 16.1.3 and 16.1.5].
At the base of the vibrissa, (5b) must hold. Thus y can be numerically computed:

$$y(s, \varphi_1^*) = \int_0^s \sin(\varphi(\tau, \varphi_1^*))\,\mathrm{d}\tau\,.$$

The shooting value for φ_1^* is correct, if $y(1, \varphi_1^*) - \eta(\alpha) = 0$.

Summarizing, independent of the chosen method, φ_1 is now known. The actual deformation and the solution of (4c,d), respectively, can be numerically computed starting at $s = 1$:

$$x = \xi(\alpha) + \int_1^s \cos(\varphi(\tau))\,\mathrm{d}\tau\,, \tag{13}$$
$$y = \eta(\alpha) + \int_1^s \sin(\varphi(\tau))\,\mathrm{d}\tau\,.$$

3.2. Phase B: Tangential Contact

The bending moment is now, with yet unknown contact point s_1 (see Fig. 11):

$$M_{bz}(s) = \begin{cases} f\Big(\big(y(s) - \eta(\alpha)\big)\sin(\alpha) + \big(x(s) - \xi(\alpha)\big)\cos(\alpha)\Big) & , s \in (0, s_1]\,, \\ 0 & , s \in (s_1, 1)\,. \end{cases} \tag{14}$$

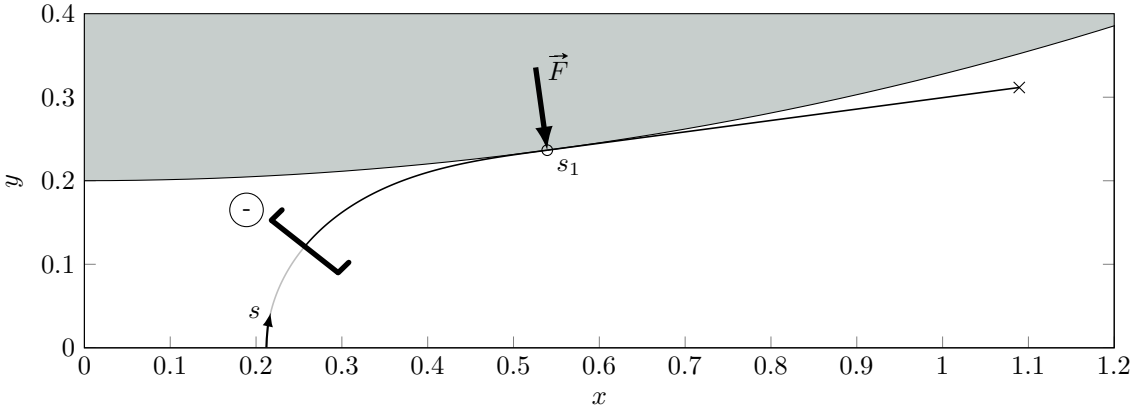

Figure 11: Deflected beam in Phase B, contact point $s_1 \in (0, 1)$.

Again the derivative of the curvature is of interest, thus the related boundary value problem is:

(a)	$\kappa'(s) = f\cos(\varphi(s) - \alpha)$	(c)	$x'(s) = \cos(\varphi(s))$	$s \in (0, s_1)$
(b)	$\varphi'(s) = \kappa(s)$	(d)	$y'(s) = \sin(\varphi(s))$	

(15)

$$\boxed{\begin{array}{llllll} \text{(a)} & \varphi(0)=\frac{\pi}{2} & \text{(c)} & \kappa(s_1)=0 & \text{(e)} & x(s_1)=\xi(\alpha) \\ \text{(b)} & y(0)=0 & \text{(d)} & \varphi(s_1)=\alpha & \text{(f)} & y(s_1)=\eta(\alpha) \end{array}} \tag{16}$$

A first integral of (15a) together with (15b) and (16c) is

$$\begin{aligned} \kappa^2 &= 2f\sin(\varphi-\alpha) \\ \Rightarrow \quad \frac{\mathrm{d}}{\mathrm{d}s}\varphi(s) &= \kappa(s) = -\sqrt{2f}\sqrt{\sin(\varphi(s)-\alpha)}\,. \end{aligned} \tag{17}$$

The ODE (15b) with (17) and (16a) yields

$$\sqrt{f}s = \mathbb{H}_B(\varphi(s)-\alpha) - \mathbb{H}_B\left(\frac{\pi}{2}-\alpha\right),$$

which can be solved for $\varphi(s)$:

$$\varphi(s) = \alpha + \mathbb{H}_B^{-1}\left(\sqrt{f}s + \mathbb{H}_B\left(\frac{\pi}{2}-\alpha\right)\right).$$

Again, fore sake of brevity, a function $\mathbb{H}_B$ is used

$$\begin{aligned} \mathbb{H}_B &: t \to \mathbb{F}\left(\sqrt{2}\sin\left(\frac{\pi}{4}-\frac{t}{2}\right), \frac{\sqrt{2}}{2}\right), \\ \mathbb{H}_B^{-1}(t) &= -\frac{\pi}{2} + 2\arccos\left(\frac{\sqrt{2}}{2}\,\text{JacobiSN}\left(t, \frac{\sqrt{2}}{2}\right)\right). \end{aligned}$$

At the contact point s_1, the slope angle $\varphi(s_1)=\alpha$ is known. Thus, the contact force can be expressed as

$$\sqrt{f} = \frac{\mathbb{H}_B(0) - \mathbb{H}_B\left(\frac{\pi}{2}-\alpha\right)}{s_1}\,. \tag{18}$$

Again, consider the function y to get the last missing parameter s_1. Condition (16b) results in:

$$\begin{aligned} y(s) &= \int_0^s \sin\left(\alpha + \mathbb{H}_B^{-1}\left(\sqrt{f}t + \mathbb{H}_B\left(\frac{\pi}{2}-\alpha\right)\right)\right)\mathrm{d}t \\ \Leftrightarrow \quad y(s) &= \frac{1}{\sqrt{f}} \int_{\mathbb{H}_B\left(\frac{\pi}{2}-\alpha\right)}^{\sqrt{f}s+\mathbb{H}_B\left(\frac{\pi}{2}-\alpha\right)} \sin\left(\alpha + \mathbb{H}_B^{-1}(\tau)\right)\mathrm{d}\tau\,. \end{aligned} \tag{19}$$

After collecting all information, (18), (19) and (16f) result in

$$f(\alpha) = \left(\frac{1}{\eta(\alpha)} \int_{\mathbb{H}_B\left(\frac{\pi}{2}-\alpha\right)}^{\mathbb{H}_B(0)} \sin\left(\alpha + \mathbb{H}_B^{-1}(\tau)\right)\mathrm{d}\tau\right)^2. \tag{20}$$

Now, (18) and (20) lead to the following equation for the contact point s_1:

$$s_1(\alpha) = \frac{\eta(\alpha)\left(\mathbb{H}_B(0) - \mathbb{H}_B\left(\frac{\pi}{2}-\alpha\right)\right)}{\displaystyle\int_{\mathbb{H}_B\left(\frac{\pi}{2}-\alpha\right)}^{\mathbb{H}_B(0)} \sin\left(\alpha + \mathbb{H}_B^{-1}(\tau)\right)\mathrm{d}\tau}\,. \tag{21}$$

The last integral of (15c) with (16e) is:

$$x(s) = x_0 + \frac{1}{\sqrt{f}} \int_{\mathbb{H}_B\left(\frac{\pi}{2}-\alpha\right)}^{\sqrt{f}s+\mathbb{H}_B\left(\frac{\pi}{2}-\alpha\right)} \cos\left(\alpha + \mathbb{H}_B^{-1}(\tau)\right)\mathrm{d}\tau\,,$$

whence, with $s = s_1$, we obtain the food coordinate

$$x_0 = \xi(\alpha) - \frac{1}{\sqrt{f}} \int_{\mathbb{H}_B\left(\frac{\pi}{2}-\alpha\right)}^{\mathbb{H}_B(0)} \cos\left(\alpha + \mathbb{H}_B^{-1}(\tau)\right) \, . \tag{22}$$

Finally, for both phases, via (13) and (22), the foot x_0 is derived. Using (11) and (20) we can determine f and, hence, knowing α, also the contact forces $\vec{F}$. With f we get the clamping force F_{Ax} and F_{Ay}, as well as the clamping moment M_{Az} using (3) or (14).

4. COMPUTATION ALGORITHM FOR THE OBSERVABLES

With the analysis done in the previous section, the next step is now numerics: the computation of the observables. The first step thereby is to find the starting point α_0 at which the beam first contacts the profile in its undeformed state: $\alpha_0 = \{\alpha \geq 0 \,|\, \eta(\alpha) = 1\}$. After this, the minimum of the function $s_{1,\text{min}} := \min(s_1(\alpha))$ at point α_{min} is determined, starting from α_0. While $s_1(\alpha)$ only produces physically realistic results in case of Phase B, it can also help to determine starting and end point of this phase. Testing Phase B, $s_{1,\text{min}} < 1$ must hold. In this case, there must exist two angles $\alpha_{B,\text{start}}$ and $\alpha_{B,\text{end}}$ at which $s_1\left(\alpha_{B,\text{start}}\right) = s_1\left(\alpha_{B,\text{end}}\right) = 1$ is valid. The graph of the function $s_1(\alpha)$ with the mentioned points is shown in Fig. 12.

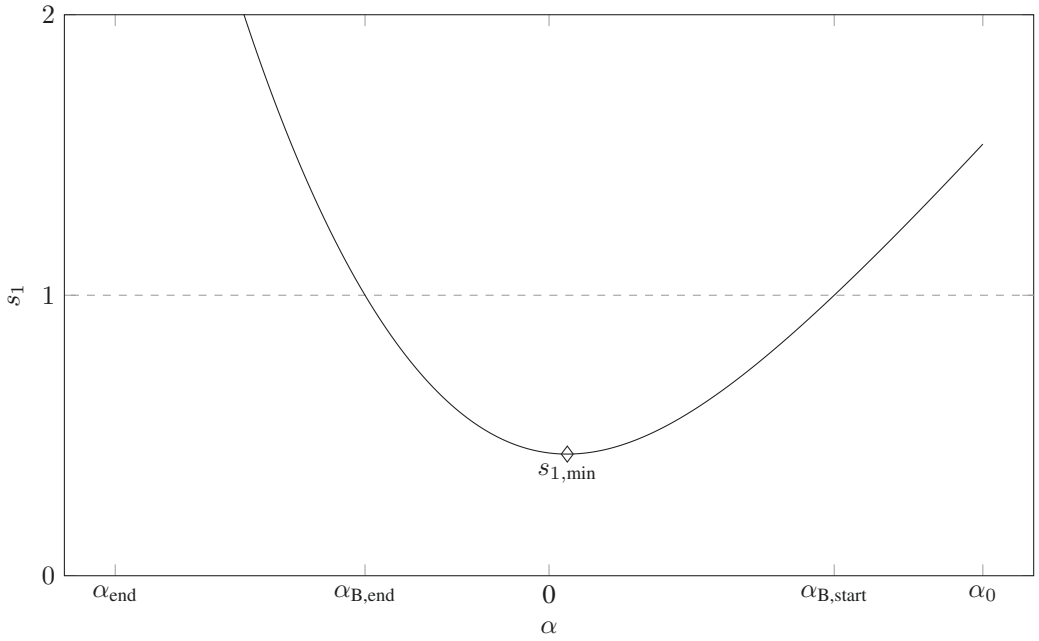

Figure 12: Graph of s_1 vs. α for profile function $g : x \mapsto \cosh\left(\frac{1}{4}x\right) - \frac{4}{5}$.

The flow chart of the proposed algorithm is shown in Fig. 13. If there is at least one point with $s_1 < 1$, the computation takes place in parallel. This can easily be done because there is no exit condition until the end of Phase B and the discrete α_k along the profiles arc length can be computed before. In case of no Phase B, the only known exit condition are reachability (can the contact point be reached with a beam of length 1) and plausibility (the base is moved from the right to the left, so $x_{0,k} > x_{0,k+1}$ must hold). Even though the case of no Phase B can also be parallelized, e.g. in a task based parallel model, the effort is higher.

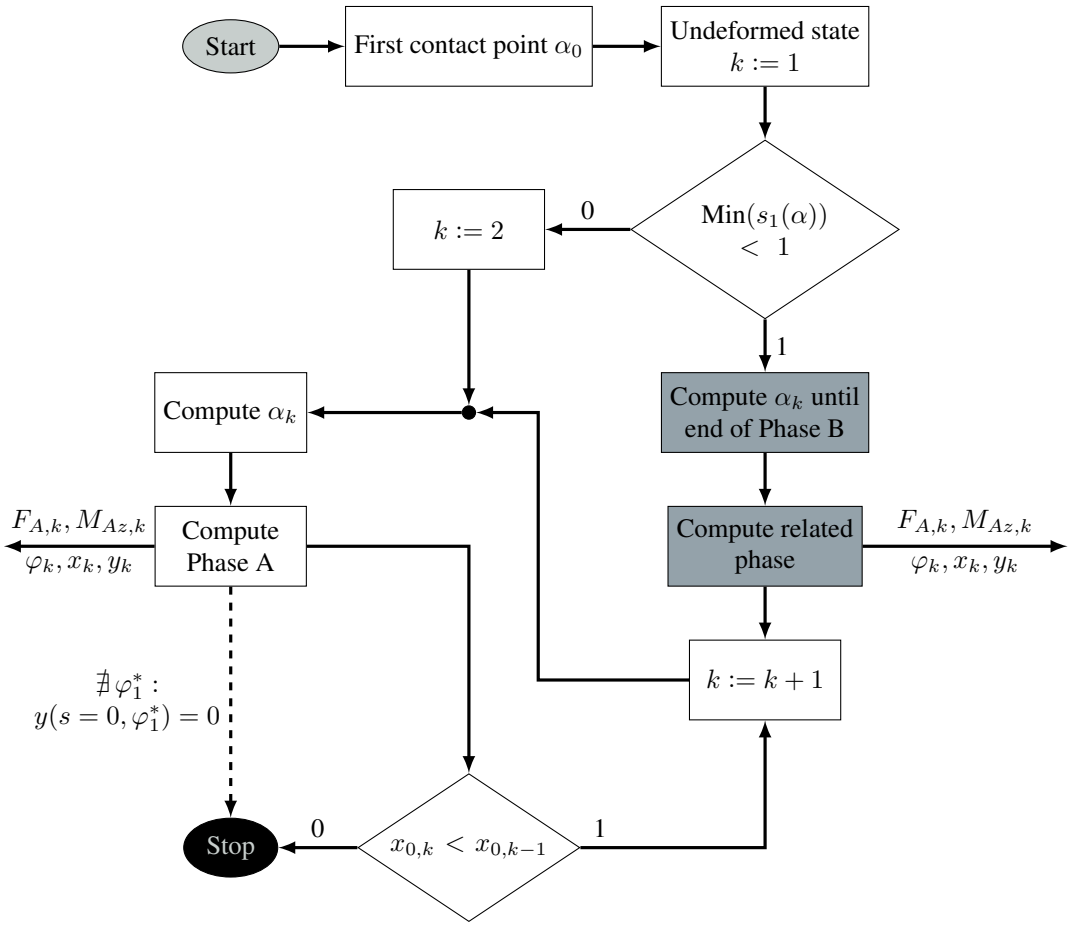

Figure 13: Flowchart for strictly convex profiles; ▭ parallel computation on PC, [13].

5. RECONSTRUCTION OF THE PROFILE

The last section dealt with the generation of observables $x_0, F_{Ax}, F_{Ay}, M_{Az}$ (values which are assumed that an animal can solely rely on) available at the base of a single vibrissa if it is swept along an obstacle. In experiments these values are governed by a measurement device.
The next step is to get information about the obstacle by using *only* the information at the base:

$$\begin{aligned}
\kappa(0) &= \lim_{s\to 0+} M_{bz}(s) = -M_{Az}\,,\\
\varphi(0) &= \frac{\pi}{2}\,,\\
x(0) &= x_0\,,\\
y(0) &= 0
\end{aligned}$$

and

$$\begin{aligned}
\alpha &= -\arctan\left(\frac{F_{Ax}}{F_{Ay}}\right)\,,\\
f &= \sqrt{F_{Ax}^2 + F_{Ay}^2}\,.
\end{aligned}$$

The main difficulty is to decide whether the actual deformation at a given point is related to Phase A or Phase B. The key to solve this is to analyze the curvature for Phases A and B, and somewhere:

$$\text{Phase A:} \qquad \kappa_A^2(s) = 2f\left(\sin(\varphi(s) - \alpha) - \sin(\varphi_1 - \alpha)\right)\,, \tag{23}$$

$$\text{any } s\text{:} \qquad \kappa_R^2(s) = 2f\sin(\varphi(s) - \alpha) - 2f\cos(\alpha) + M_{Az}^2\,, \tag{24}$$

$$\text{Phase B:} \qquad \kappa_B^2(s) = 2f\sin(\varphi(s) - \alpha)\,. \tag{25}$$

Clearly, the observables are related to Phase B if and only if $\varphi_1 = \alpha$ holds. The tip angle φ_1 can be calculated as follows:

$$\varphi_1 = \alpha - \arcsin\left(\frac{M_{Az}^2 - 2f\cos(\alpha)}{2f}\right),$$

which then results in the condition for Phase B with only known parameters:

$$\boxed{M_{Az}^2 - 2F_{Ay} = 0\,.} \tag{26}$$

If (26) is not valid, the contact force is applied at $s_1 = 1$ else the contact point s_1 must be computed:

$$s_1 = \frac{\mathbb{H}_B(0) - \mathbb{H}_B\left(\frac{\pi}{2} - \alpha\right)}{\sqrt{f}}\,.$$

The initial value problem is solved numerically using MATLAB's variable order Adams-Bashforth-Moulton PECE solver:

$$\begin{aligned}
&\varphi'(s) = -\sqrt{2f\sin(\varphi(s) - \alpha) - 2f\cos(\alpha) + M_{Az}^2}\,, && \varphi(0) = \frac{\pi}{2}\,,\\
&x'(s) = \cos(\varphi(s))\,, && x(0) = x_0\,,\\
&y'(s) = \sin(\varphi(s))\,, && y(0) = 0\,,
\end{aligned}$$

which results in the reconstructed contact point: $\xi(\alpha) = x(s_1),\ \eta(\alpha) = y(s_1)\,.$

6. SIMULATIONS

In this paper, three profile functions are presented:

$$\begin{aligned}
g_1 &: x \mapsto \cosh\left(\frac{1}{2}x\right) - \frac{4}{5}\,,\\
g_2 &: x \mapsto \frac{1}{2}x^2 + \frac{1}{2}\,,\\
g_3 &: x \mapsto \begin{cases} -\sqrt{2^2 - x^2} + \frac{5}{2}, & \alpha > 0\,,\\ -\sqrt{\frac{1}{4} - x^2} + 1, & \text{else}\,. \end{cases}
\end{aligned}$$

Function g_1 is a catenary, g_2 a parabola and g_3 a profile composed of two circles, all shown in Fig. 14. Observables and reconstruction error for profile g_1 are shown in Fig. 15. The relative error for each computation point k along the profile function g shown in Fig. 15(d) is computed using the formula

$$\text{error} := \left\| \begin{pmatrix} x_k\left(s_{1k}\right) \\ y_k\left(s_{1k}\right) \end{pmatrix} - \begin{pmatrix} \xi(\alpha) \\ \eta(\alpha) \end{pmatrix} \right\|_2$$

with s_{1k} as reconstructed contact point, $(x_k(s), y_k(s))$ the reconstructed position of the beam in the plane and $(\xi(\alpha), \eta(\alpha))$ the given contact point for computing the observables.

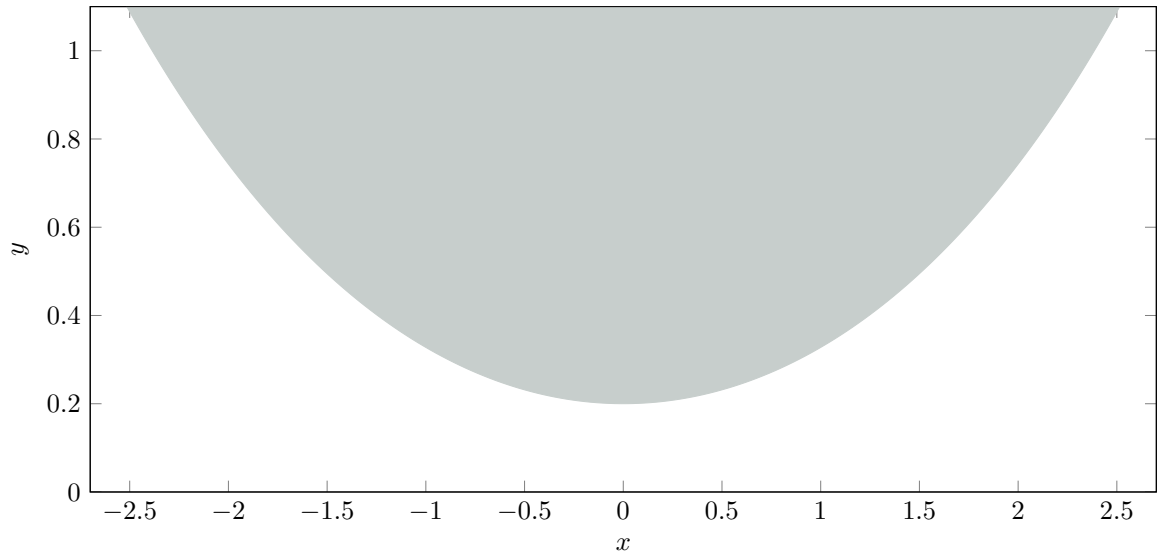

(a) Catenary profile g_1

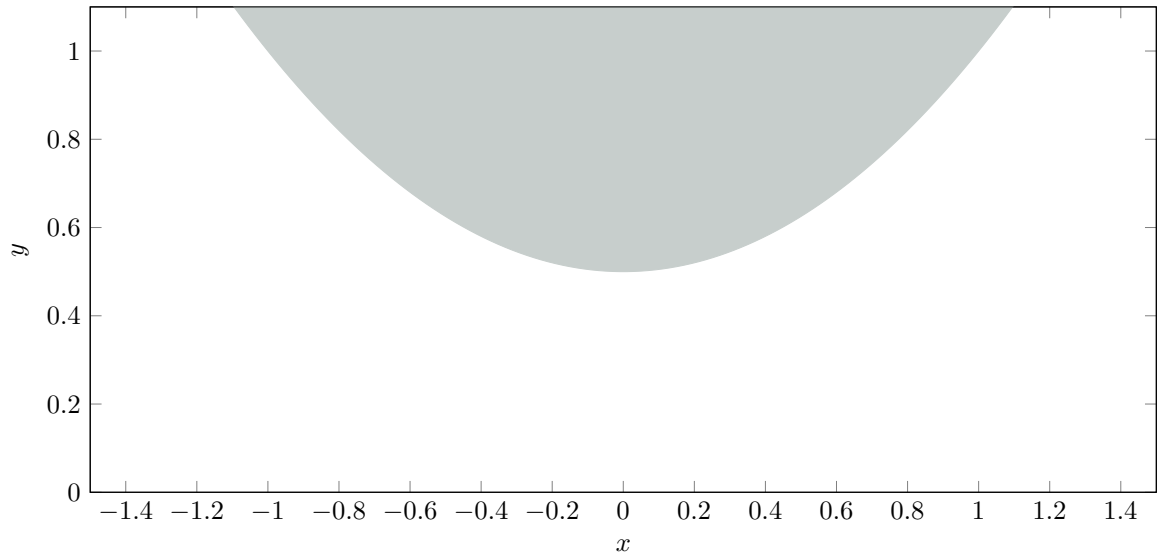

(b) Parabola profile g_2

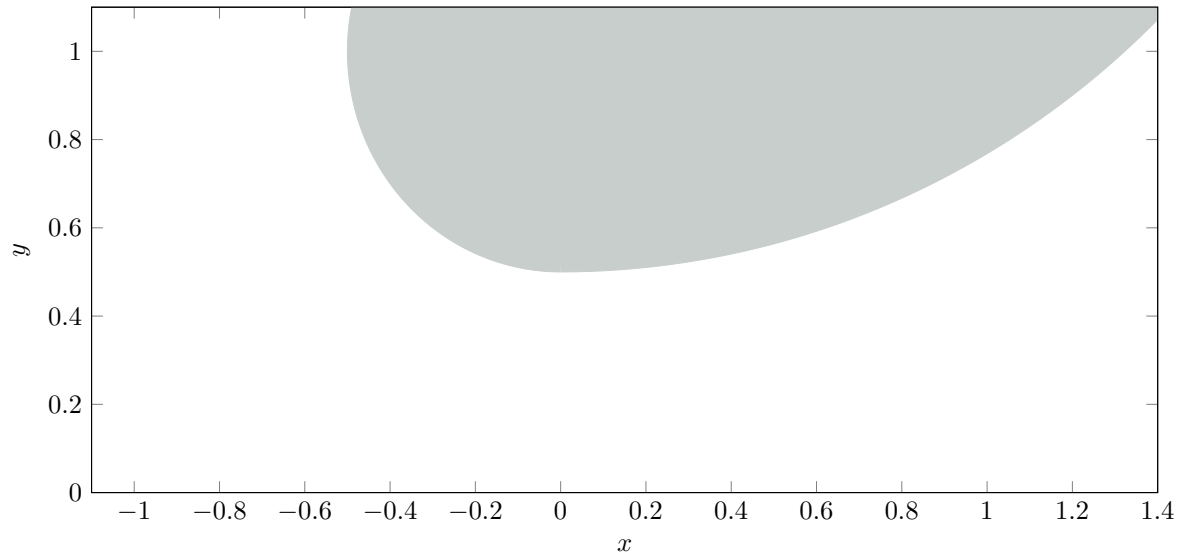

(c) Profile composed of two circles g_3

Figure 14: Profiles under consideration.

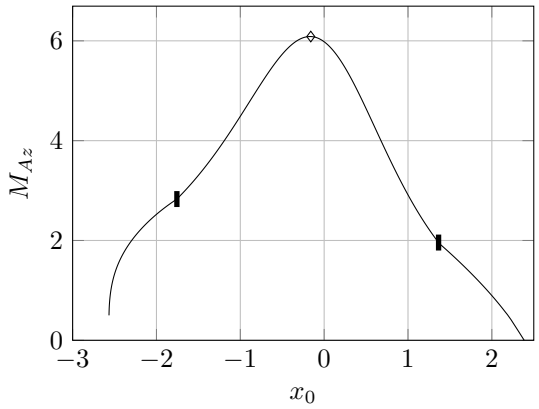

(a) Clamping moment M_{Az}

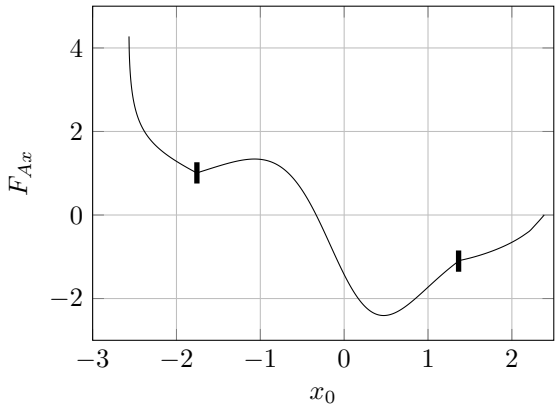

(b) Clamping force F_{Ax}

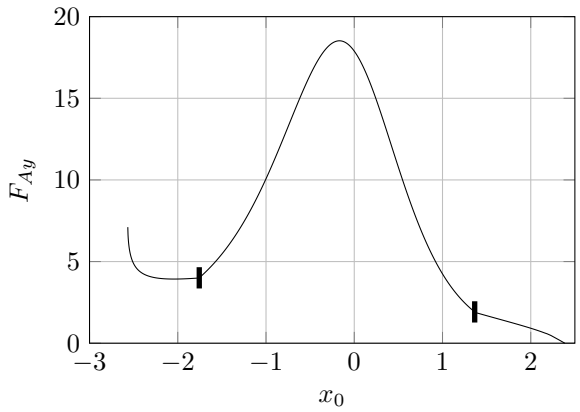

(c) Clamping force F_{Ay}

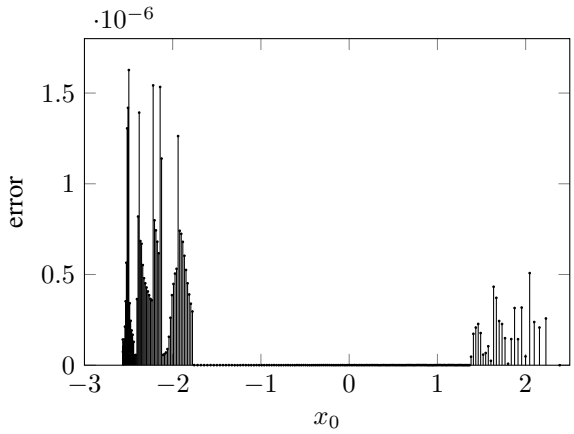

(d) Reconstruction error

Figure 15: Observables and reconstruction error with profile function g_1.

Comparison of 15(d) and 16 leads to the conclusion of the error staying within the tolerances given in the numerical computation routine to compute the observables.

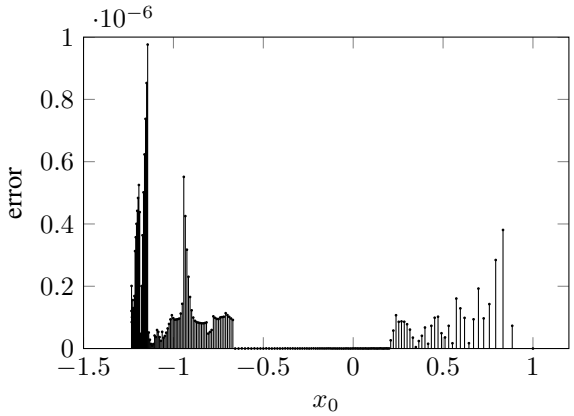

(a) Parabola profile g_2

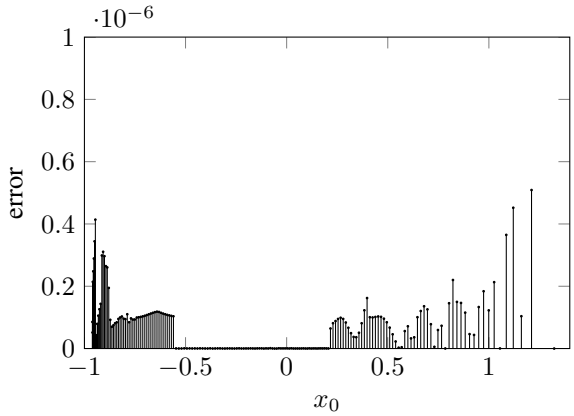

(b) Profile g_3

Figure 16: Reconstruction error.

7. CONCLUSION

From the mechanical point of view it is possible to reconstruct a profile by *sweeping one time* a thin elastic beam along it and only record forces and moments at the support. The theoretical analysis of the problem results in a very simple equation to decide if the beam contacts an object at the tip or between the tip and the base. Furthermore, a formula to calculate the contact point with respect to the arc length of the beam is provided. This analytical formula is new in literature. A reconstruction is feasible, which supports the hypothesis that animals can navigate by strongly relying on their mechanoreceptors at the FSC.
Future work should aim at increasing the level of complexity of the scanning problem and the mechanical beam sensor, respectively, as to choose $I_z = I_z(s)$, $E = E(s)$ and incorporate sliding friction and stiction during scanning.

8. REFERENCES

[1] M. Abramowitz and I. A. Stegun. *Handbook of mathematical functions: With formulas, graphs, and mathematical tables*, volume 55 of *National Bureau of Standards applied mathematics series*. United States Department of Commerce, Washington and DC, 10. print., dec. 1972, with corr edition, 1972.

[2] Carsten Behn. *Mathematical Modeling and Control of Biologically Inspired Uncertain Motion Systems with Adaptive Features*. Habilitation thesis, Ilmenau University of Technology, Ilmenau, 2013.

[3] J. A. Birdwell, J. H. Solomon, M. Thajchayapong, M. A. Taylor, M. Cheely, R. B. Towal, J. Conradt, and M. J. Z. Hartmann. Biomechanical Models for Radial Distance Determination by the Rat Vibrissal System. *Journal of Neurophysiology*, 98(4):2439–2455, 2007.

[4] T. N. Clements and C. D. Rahn. Three-dimensional contact imaging with an actuated whisker. *IEEE Transactions on Robotics*, 22(4):844–848, 2006.

[5] Leonhard Euler. *Methodus inveniendi lineas curvas maximi minimive proprietate gaudentes, sive solutio problematis isoperimetrici latissimo sensu accepti*. Bousquet, Lausannæ and Genevæ, 1744.

[6] S. Hirose, S. Inoue, and K. Yoneda. The whisker sensor and the transmission of multiple sensor signals. *Advanced Robotics*, 4(2):105–117, 1989.

[7] D. Kim and R. Möller. Biomimetic whiskers for shape recognition. *Robotics and Autonomous Systems*, 55(3):229–243, 2007.

[8] S. B. Mehta, D. Whitmer, R. Figueroa, B. A. Williams, and D. Kleinfeld. Active Spatial Perception in the Vibrissa Scanning Sensorimotor System. *PLoS Biology*, 5(2):e15, 2007.

[9] L. Pammer, D. H. O'Connor, S. A. Hires, N. G. Clack, D. Huber, E. W. Myers, and K. Svoboda. The mechanical variables underlying object localization along the axis of the whisker. *The Journal of neuroscience : the official journal of the Society for Neuroscience*, 33(16):6726–6741, 2013.

[10] G. R. Scholz and C. D. Rahn. Profile Sensing With an Actuated Whisker. *IEEE Transactions on Robotics and Automation*, 20(1):124–127, 2004.

[11] J. Steigenberger. A continuum model of passive vibrissae, 2013, TU Ilmenau, Fakultät MN, Preprint No. M 13/03. Ilmenau, Germany.

[12] C. Tuna, J. H. Solomon, D. L. Jones, and M. J. Z. Hartmann. Object shape recognition with artificial whiskers using tomographic reconstruction. In *IEEE International Conference on Acoustics, Speech and Signal Processing (ICASSP)*, pages 2537–2540, Piscataway and NJ, 2012. IEEE.

[13] Christoph Will. *Anwendung nichtlinearer Biegetheorie auf elastische Balken zur Objektabtastung am Beispiel passiver Vibrissen mit unterschiedlicher Lagerung*. Master thesis, Ilmenau University of Technology, Department of Mechanical Engineering, Ilmenau, 2013.